Interference of electric-dipole and magnetic-dipole interactions in conduction-electron-spin resonance in InSb

Y.-F. Chen,* M. Dobrowolska,† J. K. Furdyna, and S. Rodriguez
Physics Department, Purdue University, West Lafayette, Indiana 47907
(Received 7 January 1985; revised manuscript received 21 March 1985)

The contributions of the electric-dipole and magnetic-dipole matrix elements to conduction-electron-spin resonance in zinc-blende crystals are investigated theoretically and experimentally. Using time-dependent perturbation analysis, we show that these contributions interfere at the resonance condition, resulting in an anomalous dependence of the resonance intensity on the *sign* of either the dc magnetic field $\mathbf{B}_0$ or the wave vector $\mathbf{q}$ of the photon. In the context of macroscopic dielectric response, it is shown that the above interference can be represented by time-reversal symmetry associated with the wave vector. The effects of electric-dipole–magnetic-dipole (EDMD) interference at spin resonance have been studied experimentally by far-infrared (FIR) magnetotransmission in a series of InSb samples with various orientations and electron concentrations. Experiments were performed in magnetic fields up to 60 kG in both Voigt and Faraday geometries, at FIR wavelengths 96.5, 118.8, 163, and 251.1 μm, in the temperature range between 2 and 35 K. Measurements of the absorption coefficient as a function of orientation of $\mathbf{B}_0$ in (100), (110), (111), and (112) planes, and as a function of the sign of $\mathbf{B}_0$ and $\mathbf{q}$, are in excellent agreement with the predictions of the theory. These experiments provide an elegant method for determining the inversion-asymmetry parameter δ_0, yielding a value of 56 a.u. (3.6×10^{-34} erg cm^3). In addition to the EDMD interference, the FIR magnetotransmission spectra also conclusively demonstrate that the dominant mechanism allowing electric-dipole-excited spin resonance in InSb is inversion asymmetry.

I. INTRODUCTION

The possibility of observing electric-dipole-induced spin resonance (EDSR) of conduction and donor-bound electrons in semiconductors has been known for some twenty years. This transition is allowed in the presence of spin-orbit coupling, as a result of wave-function mixing through either $\mathbf{k}\cdot\mathbf{p}$ interaction[1] ("nonparabolicity"), inversion asymmetry,[2,3] or warping.[3] Of these, only inversion asymmetry allows the EDSR transition in the parallel Voigt geometry[3] ($\mathbf{E}||\mathbf{B}_0$, where $\mathbf{B}_0$ is the dc magnetic field and $\mathbf{E}$ is the electric field of the incident wave).

Our far-infrared (FIR) measurements of conduction-electron-spin resonance in *n*-type InSb indicate that EDSR is in fact stronger in the $\mathbf{E}||\mathbf{B}_0$ geometry than in the other configurations, thus establishing—contrary to earlier studies[4]—that the dominant mechanism allowing this spin-flip transition is the lack of inversion symmetry. What is more, we have observed a striking dependence of the resonance line intensity either on the *sign* of the magnetic field or on the *direction* of wave propagation with respect to the crystal axes of the sample, as illustrated by the magnetotransmission spectra shown in Figs. 1(a) and 1(b). The two figures show spin resonances of conduction and donor-bound electrons observed for opposite directions of the dc magnetic field. Comparing Figs. 1(a) and 1(b), we see that the intensity of EDSR changes quite strongly (by a factor of about 2) when the field is reversed. We found this result to be extremely surprising, because in the $\mathbf{E}||\mathbf{B}_0$ geometry the response of the medium is

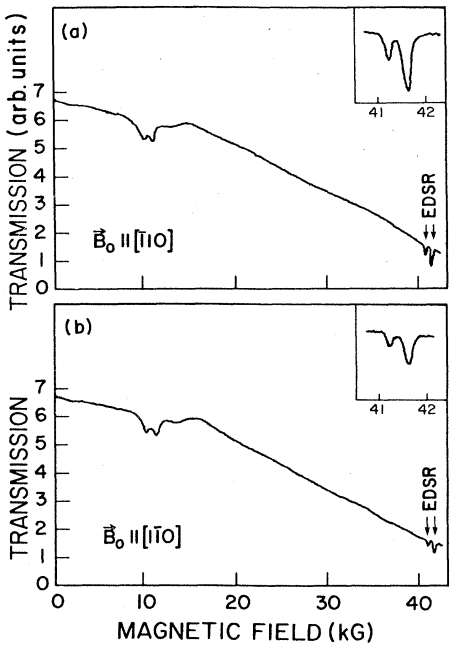

FIG. 1. Typical FIR magnetotransmission spectra for the parallel Voigt ($\mathbf{E}||\mathbf{B}_0$) configuration, obtained at 118.8 μm and 4.5 K on sample MD9 ($\mathbf{q}||[111]$). Two electric-dipole spin-resonance lines (marked EDSR in the figure and shown in insets on an expanded scale) are clearly seen. The stronger line in the doublet is the free-electron EDSR, and the weaker is the EDSR of donor-bound electrons. (a) corresponds to $\mathbf{B}||[1\bar{1}0]$. (b) is obtained by reversing $\mathbf{B}_0$ relative to (a). The scale is the same for both sets of data.

described by a diagonal element of the dielectric tensor, which by simple symmetry arguments must remain invariant under magnetic field reversal, unless the effect of the wave vector of the propagating light is included.[5]

In this paper we show, using a quantum-mechanical approach, that the observed anomalous behavior is actually a result of the interference between electric-dipole and magnetic-dipole matrix elements of the spin-resonance transition. This result is rather unexpected, because in the analysis of optical or infrared spectra the magnetic-dipole interaction is extremely weak, and is generally neglected. We find, however, that in the case of spin-flip transitions in InSb, even though the intensity of the magnetic-dipole term taken by itself is indeed small (about 2% of the intensity of the corresponding inversion-asymmetry-allowed electric-dipole transition), the *interference* of the two contributions does play an important role in the response of the medium to the incident electromagnetic wave. For example, it can change the total spin-resonance absorption coefficient by as much as a factor of 2. Using macroscopic arguments, we have shown that the above behavior can be represented by the effect of the *photon momentum* on the dielectric response function.

In addition to reporting the observation and theoretical analysis of electric-dipole—magnetic-dipole (EDMD) interference at FIR frequencies, this paper also constitutes the first systematic experimental study of the effect of inversion asymmetry on EDSR. Comparing the EDSR strength in the parallel Voigt geometry with other geometries, we conclude that inversion asymmetry is in fact the principal mechanism allowing this transition in InSb, at least in the parameter range corresponding to our experiments.

The structure of this paper is as follows. In Sec. II we develop the microscopic theory underlying the effects of EDMD interference in a zinc-blende semiconductor. In Sec. III we describe the FIR magnetotransmission apparatus and sample preparation. In Sec. IV we present the experimental results and their interpretation. Finally, the macroscopic formulation of the dielectric response function equivalent to the EDMD interference is presented in the Appendix.

II. THEORY

In this section we first demonstrate, in quantum-mechanical terms, how the EDMD interference occurs, and how it leads to an anomalous dependence of the spin-resonance (SR) absorption on the sign of either the dc magnetic field $\mathbf{B}_0$ or the wave vector $\mathbf{q}$. Next we focus on the EDMD interference in crystals with zinc-blende structure. We discuss SR for various experimental configurations (Faraday, Voigt), with special attention to the angular dependence of the absorption coefficient of SR for samples with (100), (110), (111), and (112) faces in the parallel Voigt geometry ($\mathbf{E}||\mathbf{B}_0\perp\mathbf{q}$).

A. General expression for the EDMD interference

When an electromagnetic wave with a vector potential $\mathbf{A}'$ acts on a charged particle, the perturbation Hamiltonian has the form

$$H'=\frac{e}{c}\mathbf{V}\cdot\mathbf{A}'+\frac{g\beta_0}{2}\boldsymbol{\sigma}\cdot\nabla\times\mathbf{A}' , \tag{1}$$

where $\mathbf{V}$ is the velocity operator, g is the g factor of the electron, $\beta_0=e\hbar/2m_0c$ is the Bohr magneton, m_0 is the mass of the free electron, $\boldsymbol{\sigma}=(\sigma_x,\sigma_y,\sigma_z)$ is the Pauli matrix, and $\mathbf{A}'$ is the vector potential of the electromagnetic wave,

$$\mathbf{A}'=\mathrm{Re}(\mathbf{A}'_0e^{i(\omega t-\mathbf{q}\cdot\mathbf{r})}) . \tag{2}$$

Out task is to solve the time-dependent Schrödinger equation

$$i\hbar\frac{\partial\psi}{\partial t}=(H_0+H')\psi , \tag{3}$$

where H_0 is the unperturbed Hamiltonian, which is time independent. The eigenstates of the unperturbed system are given by

$$H_0\phi_m=E_m\phi_m . \tag{4}$$

The solution for the wave function ψ may be written as

$$\psi=\sum_m a_m(t)\phi_m(\mathbf{r})e^{-iE_mt/\hbar}=\sum_m a_m\phi_m e^{-iE_mt/\hbar} . \tag{5}$$

Following elementary time-dependent perturbation theory, we obtain

$$a_m=\frac{1}{2\hbar}\frac{e}{c}\mathbf{V}_{mn}\cdot\mathbf{A}'_0\left[\frac{1-e^{i(\omega_{mn}+\omega)t}}{\omega_{mn}+\omega}+\frac{1-e^{i(\omega_{mn}-\omega)t}}{\omega_{mn}-\omega}\right]$$
$$-\frac{i}{2\hbar}\mathbf{M}_{mn}\cdot(\mathbf{q}\times\mathbf{A}'_0)$$
$$\times\left[\frac{1-e^{i(\omega_{mn}+\omega)t}}{\omega_{mn}+\omega}-\frac{1-e^{i(\omega_{mn}-\omega)t}}{\omega_{mn}-\omega}\right] , \tag{6}$$

where $\mathbf{V}_{mn}$ and $\mathbf{M}_{mn}$ are matrix elements corresponding to the electric- and magnetic-dipole terms, respectively, given by

$$\mathbf{V}_{mn}=\int\phi_m^*\mathbf{V}\phi_n d\mathbf{r}\equiv\langle m\,|\,\mathbf{V}\,|\,n\rangle , \tag{7}$$

$$\mathbf{M}_{mn}=\int\phi_m^*\mathbf{M}\phi_n d\mathbf{r}\equiv\langle m\,|\,\mathbf{M}\,|\,n\rangle , \tag{8}$$

$\mathbf{M}=g\beta_0\boldsymbol{\sigma}/2$ is the magnetic-dipole moment, and

$$\omega_{mn}=\frac{E_m-E_n}{\hbar} . \tag{9}$$

In Eq. (6) we have neglected the retardation factor by assuming that $\mathbf{A}'$ varies slowly in space. For the case of resonance, only terms which have the difference $\omega_{mn}-\omega$ in the denominator are important. The transition probability per unit time from the initial state $|n\rangle$ to a particular excited state $|n'\rangle$ is then given by

$$W=\frac{\pi}{2\hbar^2}\left|\frac{e}{c}\mathbf{V}_{n'n}\cdot\mathbf{A}'_0+i\mathbf{M}_{n'n}\cdot(\mathbf{q}\times\mathbf{A}'_0)\right|^2\delta(\omega-(\omega_{n'}-\omega_n)) , \tag{10}$$

where energy-broadening effects have been neglected. The corresponding absorption coefficient α, with the occupation factors for initial and final states included, then becomes

$$\alpha=\frac{4\pi^2 c}{\Omega n\omega\hbar}\left|\frac{e}{c}\mathbf{V}_{n'n}\cdot\hat{\xi}+i\mathbf{M}_{n'n}\cdot(\mathbf{q}\times\hat{\xi})\right|^2 \times(f_n-f_{n'})\delta(\omega-(\omega_{n'}-\omega_n)) , \tag{11}$$

where Ω is the volume of the crystal, n is the refractive index, $\hat{\xi}$ is the polarization unit vector, and f_n is the probability that state n is occupied. Expanding the above equation, we obtain

$$\alpha=\frac{4\pi^2 c}{\Omega n\omega\hbar}\left[\left|\frac{e}{c}\mathbf{V}_{n'n}\cdot\hat{\xi}\right|^2-2\,\mathrm{Re}\left[i\frac{e}{c}(\hat{\xi}\cdot\mathbf{V}_{n'n})[\mathbf{M}_{n'n}\cdot(\mathbf{q}\times\hat{\xi})]^*\right]+|i\mathbf{M}_{n'n}\cdot(\mathbf{q}\times\hat{\xi})|^2\right](f_n-f_{n'})\delta(\omega-(\omega_{n'}-\omega_n)) . \tag{12}$$

In addition to the usual absorption coefficient associated with the square of the matrix element of the electric-dipole transition, Eq. (12) contains a magnetic-dipole contribution, as well as an electric- and magnetic-dipole (EDMD) interference term. From the above equation we can see immediately that reversing the direction of propagation (which changes the sign of the wave vector $\mathbf{q}$) results in changing the sign of the interference term. It will also be shown later that reversing the direction of $\mathbf{B}_0$ changes the sign of $\mathbf{V}_{n'n}$, which has a similar effect on the interference term. Thus, because of the electric-dipole and magnetic-dipole interference, the absorption spectrum can now depend on the *sign* of either $\mathbf{B}_0$ or $\mathbf{q}$.

B. EDMD interference in zinc-blende semiconductors

We now turn to the analysis of the EDMD interference at the conduction-electron-spin-resonance condition in zinc-blende semiconductors, with particular attention given to the dependence of the effect on the sign of $\mathbf{B}_0$ and $\mathbf{q}$, and on the orientation of $\mathbf{B}_0$ and $\mathbf{q}$ relative to the crystallographic axes. The precise nature of the effects of EDMD interference—which arises from the coupling between the electric-dipole and the magnetic-dipole terms in the Hamiltonian—depends upon band-structure details of the particular material considered. For zinc-blende semiconductors the EDSR can arise from three possible sources: the lack of inversion symmetry,[2,3] wave-function mixing through $\mathbf{k}\cdot\mathbf{p}$ interaction[1] (nonparabolicity), and/or warping.[3] As will be shown in Sec. IV C, we know from experimental data that EDSR in InSb is dominated by inversion asymmetry, and we will therefore confine our analysis to that mechanism.

We use an effective-mass Hamiltonian in a magnetic field, generalized to include the term contributed by inversion asymmetry and the magnetic-dipole term. In the analysis of the anisotropy of the effect, we essentially follow the formalism developed by Rashba and Sheka,[2] but we retain the magnetic-dipole matrix element along with the electric-dipole term throughout the analysis. Retaining terms up to third order in k, the effective-mass Hamiltonian is given by[6]

$$H=\frac{\hbar^2\mathbf{k}^2}{2m^*}+\frac{g\beta_0\boldsymbol{\sigma}\cdot\mathbf{B}_0}{2}+\delta_0\boldsymbol{\sigma}\cdot\boldsymbol{\kappa} , \tag{13}$$

where m^* is the effective mass, $\hbar\mathbf{k}$ is the kinematic momentum associated with the vector potential $\mathbf{A}$ of the dc magnetic field,

$$\hbar\mathbf{k}=-i\hbar\nabla+\frac{e}{c}\mathbf{A} , \tag{14}$$

δ_0 is a parameter which is associated with the spin-orbital interaction and the inversion asymmetry, and $\boldsymbol{\kappa}$ is a vector given by

$$\kappa_x=k_y k_x k_y-k_z k_x k_z , \tag{15}$$

with the indices x, y, and z corresponding to the cubic crystal axes. κ_y and κ_z are obtained from κ_x by cyclical permutation of the indices.

A shown in Ref. 2, when the inversion asymmetry contribution in the Hamiltonian is treated as a perturbation, the matrix elements of electric-dipole spin-flip transitions have the form

$$E_d=\frac{e}{c}\sum_\alpha\langle l,-|V_\alpha|l,+\rangle =\sqrt{2}\frac{\delta_0 e^2 B_0}{c^2\hbar^2}\sum_\alpha\frac{-\beta^*}{q_\alpha-\beta^*}B_{(\alpha 12)}(2l+1-2\zeta^2) , \tag{16}$$

for an arbitrary magnetic field orientation and arbitrary polarization. Here l is the Landau-level quantum number of the initial and final states; $\alpha=1,2,3$ is the polarization index corresponding to left-circular [cyclotron-resonance-active (CRA)], right-circular [cyclotron-resonance-inactive (CRI)], and parallel Voigt ($\mathbf{E}||\mathbf{B}_0$) polarizations, respectively; and q_α is the change in Landau quantum number under the action of the operator a_α, where

$$a_1=\left[\frac{c\hbar}{2eB_0}\right]^{1/2}(k_x-ik_y) ,$$

$$a_2=\left[\frac{c\hbar}{2eB_0}\right]^{1/2}(k_x+ik_y) ,$$

$$a_3=\left[\frac{c\hbar}{eB_0}\right]^{1/2}k_z\equiv\zeta$$

(i.e., a_1 and a_2 are lowering and raising operators, respectively, for inter-Landau-level transitions). Thus $q_\alpha=-1$, 1, or 0 as $\alpha=1$, 2, or 3, respectively. Further, $\beta^*=m^*g/2m_0$ is the ratio of the spin splitting to the cyclotron spacing, and $B_{(\alpha 12)}$ are trigonometric functions of the angle between the crystal axes and $\mathbf{B}_0$, derived in Ref. 2. These functions—which contain all information concerning the anisotropy of the matrix element for electric dipole transitions—are as follows:

$$B_{(112)}=-\tfrac{1}{2}\cos(2\phi)\cos(2\theta)+\frac{i}{4}\sin(2\phi)\cos\theta(2\cos^2\theta-\sin^2\theta)\ ,$$

$$B_{(212)}=\frac{3i}{4}\sin(2\phi)\sin\theta\sin(2\theta)\ , \tag{17}$$

$$B_{(312)}=\frac{-3i}{4\sqrt{2}}[\cos(2\phi)\sin(2\theta)-i\sin(2\phi)\sin\theta(2\cos^2\theta-\sin^2\theta)]\ ,$$

where θ and ϕ are the polar and azimuthal angle of the magnetic field $\mathbf{B}_0$, respectively. Note that the matrix element of V_α in Eq. (16) is *linear* in B_0; i.e., it changes sign when the direction of $\mathbf{B}_0$ is reversed, as has already been mentioned.

Proceeding similarly as in the calculation for the electric-dipole transition, we obtain the matrix element for the magnetic-dipole term,

$$M_d=\frac{i}{2}g\beta_0\langle l,-|\sigma_\alpha|l,+\rangle(\mathbf{q}\times\hat{\boldsymbol{\xi}})_\alpha=\frac{i\sqrt{2}}{2}g\beta_0(\mathbf{q}\times\hat{\boldsymbol{\xi}})_\alpha\delta_{\alpha 2}\ . \tag{18}$$

In this expression M_d (which depends on the components of the magnetic field of the incident wave expressed in the coordinate system where $\hat{\mathbf{z}}\|\mathbf{B}_0$) is not necessarily isotropic, and may contain both real and imaginary parts. This feature is a consequence of the particular choice of coordinates. However, the resonance intensity, which is proportional to $|M_d|^2$, is isotropic—i.e., independent of θ and ϕ—for all the principal geometries, as would be expected. We will examine these properties in a later section.

Substituting Eqs. (16) and (18) into Eq. (12), we obtain the absorption coefficient for the spin resonance, including the EDMD interference term, for a zinc-blende crystal:

$$\alpha=\frac{4\pi^2c}{\Omega n\omega\hbar}\left[\left|\sqrt{2}\frac{\delta_0}{\hbar}\frac{e^2B_0}{c^2\hbar}\frac{-\beta^*}{q_\alpha-\beta^*}B_{(\alpha 12)}(2l+1-2\zeta^2)\right|^2-2\,\mathrm{Re}\left[\frac{i\delta_0}{\hbar}\frac{e^2B_0}{c^2\hbar}\frac{-\beta^*}{q_\alpha-\beta^*}g\beta_0B_{(\alpha 12)}(2l+1-2\zeta^2)(\mathbf{q}\times\hat{\boldsymbol{\xi}})_2^*\right]+\left|\frac{i\sqrt{2}}{2}g\beta_0(\mathbf{q}\times\hat{\boldsymbol{\xi}})_2\right|^2\right](f_{l,+}-f_{l,-})\delta(\omega-(\omega_{l,-}-\omega_{l,+}))\ . \tag{19}$$

For a pure InSb sample (i.e., one with sufficiently low electron concentration) in a high magnetic field, the electrons are in the ground state $|0,+\rangle$ before perturbation. We can assume this to hold in the case of our measurements. We shall also neglect the small contribution $2\zeta^2=2(c\hbar/eB_0)k_z^2$ with respect to unity. The absorption coefficient then simplifies to

$$\alpha=\frac{4\pi^2cN}{n\omega\hbar}\left[\left|\sqrt{2}\frac{\delta_0e^2B_0}{c^2\hbar^2}\frac{-\beta^*}{q_\alpha-\beta^*}B_{(\alpha 12)}\right|^2-2\,\mathrm{Re}\left[\frac{i\delta_0e^2B_0}{\hbar^2c^2}\frac{-\beta^*}{q_\alpha-\beta^*}g\beta_0B_{(\alpha 12)}(\mathbf{q}\times\hat{\boldsymbol{\xi}})_2^*\right]+\left|\frac{i\sqrt{2}}{2}g\beta_0(\mathbf{q}\times\hat{\boldsymbol{\xi}})_2\right|^2\right]\delta(\omega-(\omega_{l,-}-\omega_{l,+}))\ , \tag{20}$$

where N is the free carrier concentration. If the energy states are broadened to some degree, we may replace the δ function by a normalized broadening function, i.e.,

$$\delta(\omega-(\omega_{l,-}-\omega_{l,+}))\rightarrow\frac{\gamma/2\pi}{[\omega-(\omega_{l,-}-\omega_{l,+})]^2+\gamma^2/4}\ , \tag{21}$$

where γ is a phenomenological broadening constant. At spin resonance ($\omega=\omega_{l,-}-\omega_{l,+}$) the absorption coefficient then takes the form

$$\alpha=\frac{8\pi cN}{n\omega\hbar\gamma}\left[\left|\sqrt{2}\frac{\delta_0e^2B_0}{c^2\hbar^2}\frac{-\beta^*}{q_\alpha-\beta^*}B_{(\alpha 12)}\right|^2+2\,\mathrm{Re}\left[\frac{i\delta_0e^2B_0}{\hbar^2c^2}\frac{-\beta^*}{q_\alpha-\beta^*}g\beta_0B_{(\alpha 12)}(\mathbf{q}\times\hat{\boldsymbol{\xi}})_2^*\right]+\left|\frac{i\sqrt{2}}{2}g\beta_0(\mathbf{q}\times\hat{\boldsymbol{\xi}})_2\right|^2\right]$$

$$=\frac{8\pi cN}{n\omega\hbar\gamma}[|E_d|^2+2\,\mathrm{Re}(E_dM_d^*)+|M_d|^2]\ . \tag{22}$$

In Eq. (22) we have assumed that the broadening parameter γ is the same for the electric- and the magnetic-dipole transitions. This assumption is physically justified because the above formulation is for a single electron undergoing the *same* transition (and therefore experiencing the same level broadening) under the simultaneous action of an electric and a magnetic field.

Using Eq. (22), we shall now examine the EDMD interference in the principal experimental configurations.

C. EDMD interference in specific geometries

1. Faraday geometry

The Faraday geometry refers to the configuration where wave propagation is parallel to the dc magnetic field. In this case there are two normal modes which can be supported by the medium, the cyclotron-resonance-active (CRA) polarization, i.e., that circular polarization which excites cyclotron resonance of conduction electrons, and the cyclotron-resonance-inactive (CRI) polarization. For the CRA polarization there is no magnetic-dipole transition because $g<0$, and the EDMD interference will therefore vanish for this mode. In the CRI polarization, the matrix element for the electric-dipole transition at sufficiently low electron concentrations and high magnetic fields (so that only the ground state is occupied) is

$$E_d=\sqrt{2}\frac{\delta_0 e^2 B_0}{\hbar^2 c^2}\frac{\beta^*}{\beta^*-1}B_{(212)} =\frac{i3\sqrt{2}}{4}\frac{\delta_0 e^2 B_0}{\hbar^2 c^2}\frac{\beta^*}{\beta^*-1}\sin(2\phi)\sin\theta\sin(2\theta)\ . \quad (23)$$

From Eq. (18), the matrix element for the magnetic-dipole transition for CRI excitation is

$$M_d=\frac{\sqrt{2}}{2}g\beta_0 q\ , \quad (24)$$

where $q=\omega n/c$ is the wave vector *inside* the medium, n being the index of refraction. We immediately see that for this polarization M_d and E_d are always out of phase (one is imaginary while the other one is real), and the interference again vanishes.

We thus conclude that there is no EDMD interference at spin resonance in the Faraday geometry, and consequently the spectrum does not depend on the sign of $\mathbf{B}_0$ or $\mathbf{q}$. (Note that $\mathbf{B}_0$ reversal of course changes CRA to CRI in the Faraday geometry. What we mean here is that there is no change in the spin-resonance intensity when $\mathbf{B}_0$ and the circular polarization are reversed simultaneously, or when the sample is flipped front to back.)

2. Voigt geometry

The configuration where the propagation of the wave is perpendicular to the dc magnetic field is referred to as the Voigt geometry. There are two independent modes which can be supported by the medium in this geometry: the parallel, or ordinary Voigt geometry (OV), where the electric field is parallel to the dc magnetic field (and the magnetic field $\mathbf{H}'$ of the wave is perpendicular to $\mathbf{B}_0$); and the perpendicular, or extraordinary Voigt geometry (EV), where the electric field is perpendicular to $\mathbf{B}_0$, and the magnetic field of the wave is parallel to $\mathbf{B}_0$.

We see immediately that the EV geometry does not manifest magnetic-dipole spin resonance because there $\mathbf{H}'\|\mathbf{B}_0$, so that $M_d=0$, and hence the interference also disappears. The OV geometry, on the other hand, turns out to be most interesting in the spin-resonance context, and we will investigate it in detail. In particular, we shall examine the angular dependence of spin resonance in this geometry for the dc magnetic field in the (110), (100), (111), and (112) planes.

From Eqs. (16) and (17), the matrix element for the EDSR transition in the OV geometry, for the magnetic field in an arbitrary plane, is given by

$$E_d=\sqrt{2}\frac{\delta_0 e^2 B_0}{\hbar^2 c^2}B_{(312)} =-\frac{3}{4}i\frac{\delta_0 e^2 B_0}{\hbar^2 c^2}[\cos(2\phi)\sin(2\theta) -i\sin(2\phi)\sin\theta(2\cos^2\theta-\sin^2\theta)]\ . \quad (25)$$

Using Eq. (25), we now consider EDSR for the magnetic field $\mathbf{B}_0$ in specific planes.

$\mathbf{B}_0$ in the (110) plane: An arbitrary orientation of the dc magnetic field $\mathbf{B}_0$ in the (110) plane is described by $\phi=45°$, and θ ranging from 0 to 2π. Substituting $\phi=45°$ into Eq. (25), we have

$$E_d=-\frac{3}{4}\frac{\delta_0 e^2 B_0}{\hbar^2 c^2}\sin\theta(2\cos^2\theta-\sin^2\theta)\ . \quad (26)$$

From Eq. (18), the matrix element for the magnetic-dipole transition is

$$M_d=\frac{g\beta_0 q}{2}\ , \quad (27)$$

where $q=\omega n/c$. Comparing Eqs. (26) and (27), we note that both matrix elements are real (both are in phase), and EDMD interference will therefore occur. Substituting Eqs. (26) and (27) into Eq. (22), the resulting absorption coefficient is given by

$$\alpha=\frac{8\pi cN}{n\omega\hbar\gamma}\left[\left[-\frac{3}{4}\frac{\delta_0 e^2 B_0}{\hbar^2 c^2}\sin\theta(2\cos^2\theta-\sin^2\theta)\right]^2-\frac{3}{4}\frac{\delta_0 e^2 B_0 g\beta_0 q}{\hbar^2 c^2}\sin\theta(2\cos^2\theta-\sin^2\theta)+\left[\frac{g\beta_0 q}{2}\right]^2\right]\ . \quad (28)$$

In this expression, the first term describes the contribution of EDSR alone, the second term represents the EDMD interference (its sign depending on the signs of $\mathbf{B}_0$ and $\mathbf{q}$), and the third term shows the isotropic contribution of the magnetic-dipole absorption. In Fig. 2(a) we show the angular dependence of α caused by the electric dipole alone and magnetic dipole alone. Figure 2(b) shows the total α as given by Eq. (28), including the EDMD interference. The horizontal axis in Fig. 2 is the angle between the $[1\bar{1}0]$ direction and $\mathbf{B}_0$ in the (110) plane. The bottom straight line in Fig. 2(a) shows the isotropy of the magnetic-dipole spin-resonance absorption. Figure 2(a) also shows the 180° symmetry for the electric-dipole transition, i.e., reversing the magnetic field with respect to the crystal axes yields the same absorption. However, Fig. 2(b) does not restore the value of α when the sample is rotated by 180° about $\mathbf{q}$ (or when the field is reversed). Comparing Figs. 2(a) and 2(b), we thus see that the EDMD interference strongly affects the angular dependence of the absorption coefficient, and leads to the dependence of the absorption on the sign of the magnetic field with respect to the crystal axes. Figure 2 uses parameters such that the ratio between the magnetic-dipole resonance intensity (if it occurred alone) and the maximum electric-dipole resonance intensity is about 2%. Thus, even when the magnetic-dipole interaction is itself very weak, it does play an important role in the spin-resonance spectrum through interference with the electric-dipole interaction.

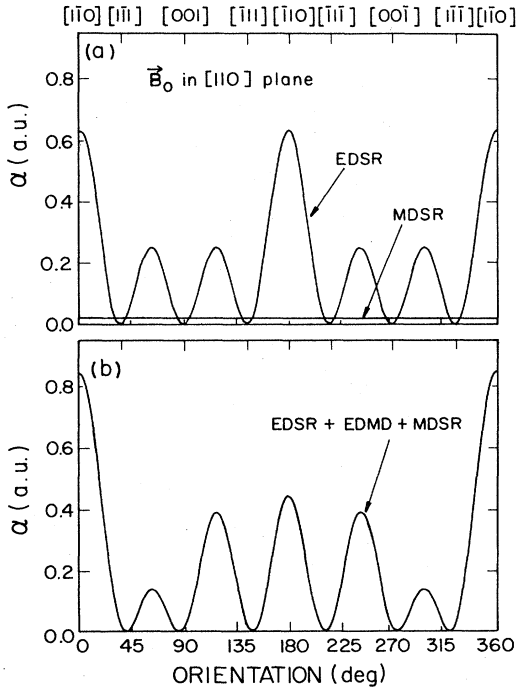

FIG. 2. Calculated absorption coefficient α of spin resonance calculated as a function of orientation of $\mathbf{B}_0$ in the (110) plane. (a) shows the relative intensities for the electric-dipole (EDSR) and magnetic-dipole (MDSR) spin resonances, calculated separately. (b) shows the *total* spin-resonance absorption coefficient, including the EDMD interference.

The interference provides a direct method for obtaining the parameters associated with inversion asymmetry. In EDSR itself the anisotropy, which is purely a trigonometric function, does not provide a measure of δ_0. In the presence of EDMD interference, however, both δ_0 and δ_0^2 terms enter into the angular dependence of the absorption. Thus, by reversing the magnetic field $\mathbf{B}_0$ and measuring the ratio of the respective absorption coefficients α, we are able to obtain an accurate value of δ_0, independent of other parameters, such as sample thickness, electron concentration, or the broadening parameter γ. For instance, if $\mathbf{B}_0$ is parallel or antiparallel to the $[1\bar{1}0]$ direction, and the ratio of the absorption coefficients for the two orientations is R, δ_0 is related to R by the expression

$$\delta_0=\frac{2(\sqrt{R}+1)g^2\beta_0^2nc\hbar}{3(\sqrt{R}-1)e^2}\ , \tag{29a}$$

which in atomic units (i.e., $\hbar=m_0=e=1$) becomes

$$\delta_0=\frac{1}{6}\frac{(\sqrt{R}+1)}{(\sqrt{R}-1)}g^2n\alpha_{\rm FS}\ \text{a.u.}, \tag{29b}$$

where $\alpha_{\rm FS}=\frac{1}{137}$ is the fine-structure constant.

B_0 in (100) plane: Magnetic field $\mathbf{B}_0$ in the (100) plane corresponds to $\phi=90°$ and θ ranging from 0 to 2π. Substituting $\phi=90°$ into Eq. (25), we obtain the matrix element for the EDSR transition

$$E_d=-i\frac{3}{4}\frac{\delta_0e^2B_0}{\hbar^2c^2}\sin(2\theta)\ . \tag{30}$$

As for $\mathbf{B}_0$ in the (110) plane, the matrix element for the magnetic-dipole transition is

$$M_d=\frac{g\beta_0q}{2}\ . \tag{31}$$

The magnetic-dipole and electric-dipole matrix elements are therefore out of phase, which leads to the disappearance of the EDMD interference for this case.

Substituting Eqs. (30) and (31) into Eq. (22), the total absorption coefficient for this plane is given by

$$\alpha=\frac{8\pi cN}{n\omega\hbar\gamma}\left[\left[\frac{3}{4}\frac{\delta_0e^2B_0}{\hbar^2c^2}\sin(2\theta)\right]^2+\left[\frac{g\beta_0q}{2}\right]^2\right]\ . \tag{32}$$

In this expression α is simply the sum of the electric-dipole absorption and the magnetic-dipole absorption, taken independently. The presence of the magnetic dipole shifts the absorption coefficient upwards by a very small amount, but does not affect its angular dependence, as shown in Fig. 3. The coefficient α thus preserves its 180° symmetry, and the absorption spectrum does *not* change when either the magnetic field or the direction of propagation is reversed.

B_0 in (111) or (112) planes: To describe an arbitrary orientation of $\mathbf{B}_0$ in either the (111) or the (112) plane, ϕ is no longer a fixed angle, as was the case for the (100) and (110) planes. Instead, ϕ and θ have to satisfy the following constraints: For $\mathbf{B}_0$ in the (111) plane:

$$\cos\theta=(\tfrac{1}{3})^{1/2}\sin\beta_{(111)}\ , \tag{33}$$

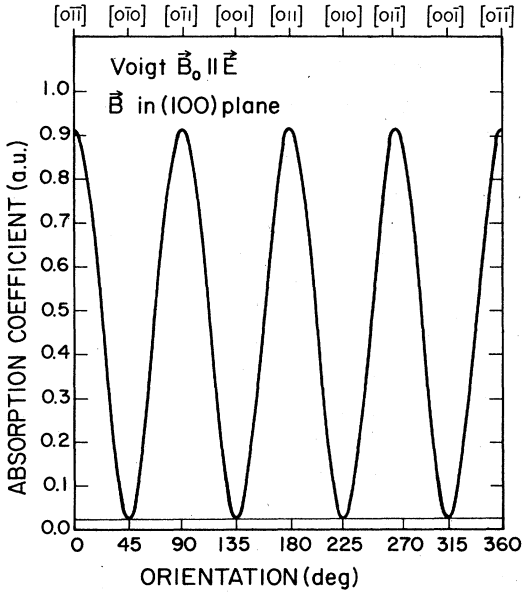

FIG. 3. Calculated spin-resonance absorption coefficient α as a function of orientation of $\mathbf{B}_0$ in the (100) plane. The thick curve shows the total absorption coefficient. The horizontal line shows the magnetic-dipole spin-resonance contribution alone. EDMD interference is absent when $\mathbf{B}_0$ is in this plane.

$$\tan\phi=\frac{\sqrt{2}\cos\beta_{(111)}+(\frac{2}{3})^{1/2}\sin\beta_{(111)}}{\sqrt{2}\cos\beta_{(111)}-(\frac{2}{3})^{1/2}\sin\beta_{(111)}}\ , \tag{34}$$

and for $\mathbf{B}_0$ in the (112) plane:

$$\cos\theta=\frac{1}{\sqrt{3}}\sin\beta_{(112)}\ , \tag{35}$$

$$\tan\phi=\frac{\sqrt{3}\cos\beta_{(112)}+\sqrt{2}\sin\beta_{(112)}}{\sqrt{3}\cos\beta_{(112)}-\sqrt{2}\sin\beta_{(112)}}\ , \tag{36}$$

where $\beta_{(111)}$ and $\beta_{(112)}$ are the angles between the $[1\bar{1}0]$ direction and $\mathbf{B}_0$ in the (111) and the (112) plane, respectively. Thus, for $\mathbf{B}_0$ in these two planes, the matrix elements for the electric-dipole transition are obtained by substituting the appropriate angles, Eqs. (33)—(36), into Eq. (25). Similarly, the matrix element for the magnetic-dipole transition is obtained from Eq. (18). For $\mathbf{B}_0$ in the (111) plane, M_d is given by

$$M_d=i\frac{g\beta_0}{2}q\frac{1}{\sqrt{3}}[\cos\theta(\sin\phi-\cos\phi)+\sin\theta +i(\sin\phi+\cos\phi)]\ , \tag{37}$$

and for $\mathbf{B}_0$ in the (112) plane the result is

$$M_d=i\frac{g\beta_0}{2}q\frac{1}{\sqrt{6}}[\cos\theta(\sin\phi-\cos\phi)+2\sin\theta +i(\sin\phi+\cos\phi)]\ . \tag{38}$$

The resonance intensity for the magnetic dipole alone is proportional to $|M_d|^2$, which is isotropic, as would be expected.

Thus, the magnetic-dipole and the electric-dipole matrix elements both contain real and imaginary parts. There will then be interference between the in-phase terms, i.e., $\mathrm{Re}(E_d)$ will interfere with $\mathrm{Re}(M_d)$—as was the case for the (110) face—and $\mathrm{Im}(E_d)$ will interfere with $\mathrm{Im}(M_d)$. The total absorption coefficient for the spin resonance, including the EDMD interference, are given below: For $\mathbf{B}_0$ in the (111) plane

$$\alpha=\frac{8\pi cN}{n\omega\hbar\gamma}\left[\left(\frac{3}{4}\frac{\delta_0 e^2B_0}{\hbar^2c^2}\right)^2\{[\cos(2\phi)\sin(2\theta)]^2+[\sin(2\phi)\sin\theta(2\cos^2\theta-\sin^2\theta)]^2\} +\frac{3}{4\sqrt{3}}\frac{\delta_0e^2B_0}{c^2\hbar^2}g\beta_0q\{\cos(2\phi)\sin(2\theta)[\cos\theta(-\sin\phi+\cos\phi)-\sin\theta] +\sin(2\phi)\sin\theta(2\cos^2\theta-\sin^2\theta)(\cos\phi+\sin\phi\}+\left(\frac{g\beta_0q}{2}\right)^2\right]\ ; \tag{39}$$

and for $\mathbf{B}_0$ in the (112) plane

$$\alpha=\frac{8\pi cN}{n\omega\hbar\gamma}\left[\left(\frac{3}{4}\frac{\delta_0 e^2B_0}{c^2\hbar^2}\right)^2\{[\cos(2\phi)\sin(2\theta)]^2+[\sin(2\phi)\sin\theta(2\cos^2\theta-\sin^2\theta)]^2\} +\frac{3}{4\sqrt{6}}\frac{\delta_0e^2B_0}{c^2\hbar^2}g\beta_0q\{\cos(2\phi)\sin(2\theta)[\cos\theta(-\sin\phi+\cos\phi)-2\sin\theta] +\sin(2\phi)\sin\theta(2\cos^2\theta-\sin^2\theta)(\cos\phi+\sin\phi)\}+\left(\frac{g\beta_0q}{2}\right)^2\right]\ . \tag{40}$$

In Eqs. (39) and (40) the first term represents the absorption coefficient for "bare" EDSR, the second term is the contribution of the EDMD interference, and the third term gives the isotropic magnetic-dipole spin-resonance absorption.

Here we have only analyzed crystals of the zinc-blende type. Extending these considerations to other types of acentric crystals (e.g., wurtzite) should lead to similar results. In view of the recent observation of EDSR in $Cd_{1-x}Mn_xSe$,[7] such analysis would be useful and timely.

III. EXPERIMENTAL PROCEDURE AND SAMPLE PREPARATION

The characteristics of the *n*-type InSb samples used in these experiments are listed in Table I. Carrier concentrations were obtained from far-infrared (FIR) Fabry-Perot oscillations,[8] and confirmed by microwave helicon interferometry.[9] Each sample was oriented by the standard Laue x-ray technique, cut on a diamond-wire saw such that the sample faces were parallel to a desired crystal plane, and then cut in the form of a 7-mm-diam disk. The surfaces of the disk samples were ground in succession with 600- and 1200-grit carborundum powder, and then polished on a microcloth saturated with a suspension of 5-μm alumina powder in distilled water. After polishing, the orientation of the samples was again checked and found to be within 2° of the specified orientation.

For III-V compounds with zinc-blende structure, the polarity along the [111] directions leads to pronounced physico-chemical differences between the (111) surfaces terminating in group-III atoms and those terminating in group-V atoms.[10,11] A 3-sec etch in a solution of 2 parts HF, 1 part HNO_3, and 1 part CH_3COOH applied to the InSb samples reveals etch pits on the (111), or In, face and no etch pits on the $(\bar{1}\bar{1}\bar{1})$, or Sb, face. Thus, for our measurements it is possible to distinguish physically between the [111] and $[\bar{1}\bar{1}\bar{1}]$ directions by etching, and hence to determine the direction of the magnetic field and the wave vector with respect to the zinc-blende lattice in *absolute* terms. This in turn, as will be seen, permits systematic comparison of spin-resonance anisotropy data obtained on different samples.

Far-infrared magnetotransmission measurements were performed at liquid-helium temperatures, at a series of fixed wavelengths ($\lambda=96.5$, 118.8, 163, and 251.1 μm). The source of the radiation was an optically pumped FIR laser (Apollo Lasers, Inc., model no. 118), with CH_3OH as the lasing gas filling the FIR cavity. The samples were mounted in a Janis "supervaritemp" optical Dewar at the center of a split-coil superconducting solenoid with a maximum magnetic field of 60 kG. The transmitted FIR signal was detected by a carbon bolometer placed directly behind the sample. A lock-in amplifier with a 16-Hz chopper and an *XY* plotter were used to amplify and record the signal. The measurements were carried out in both the Voigt and the Faraday geometries, using linearly polarized waves ($\mathbf{E}||\mathbf{B}_0$ and $\mathbf{E}\perp\mathbf{B}_0$) in the former, and circularly polarized waves (CRA and CRI) in the latter configuration. Circular polarizations were produced using quarter-wave plates ground from *xy* cut crystalline quartz.

IV. RESULTS AND DISCUSSION

A. Dependence of spin-resonance absorption on the sign of $\mathbf{B}_0$ and $\mathbf{q}$

The unusual behavior of InSb magnetotransmission spectra at spin resonance observed on reversing $\mathbf{B}_0$ or $\mathbf{q}$ in the parallel Voigt geometry is illustrated by the data shown in Fig. 4, obtained on a sample with $(1\bar{1}0)$ faces in a sequence of configurations.[5] Figure 4(a) shows the SR signal for $\mathbf{B}_0||[110]$ (in the face of the sample), with $\mathbf{q}||[1\bar{1}0]$ (normal to the sample). Figure 4(b) shows SR when the sample is rotated by 180° about $\mathbf{q}$ with respect to Fig. 4(a). Figure 4(c) is for the sample rotated by 180° about $\mathbf{B}_0$ relative to Fig. 4(a) (i.e., flipped front to back about the [110] axis), without changing the direction of $\mathbf{q}$ in the laboratory frame. Figure 4(d) is observed for the sample rotated by 180° about $\mathbf{q}\times\mathbf{B}_0$ relative to Fig. 4(a) (in this case, flipped front to back about the [001] cubic axis). Figures 4(a')—4(d') show spin resonance observed with the field reversed relative to Figs. 4(a)—4(d), respectively. The scale is identical for all data in Fig. 4. The following features emerge from the figure.

TABLE I. Sample parameters.

Sample No.	Carrier concentration (cm^{-3}) (FIR)	Carrier concentration (cm^{-3}) (helicons)	Thickness (mm)	Orientation
W-3106-*C*	1.6×10^{14}	1.3×10^{14}	2.07	(112)
MD1	9.0×10^{14}	9.0×10^{14}	2.49	(112)
MD4	4.7×10^{15}	4.2×10^{15}	1.98	(110)
MD5	4.5×10^{15}	4.7×10^{15}	1.98	(100)
MD6	4.5×10^{15}	3.9×10^{15}	3.00	(111)
MD7	2.3×10^{14}	2.7×10^{14}	4.52	(110)
MD8	3.6×10^{14}	2.0×10^{14}	3.95	(100)
MD9	4.5×10^{14}	5.0×10^{14}	3.94	(111)
MD10	6.8×10^{14}	7.1×10^{14}	1.87	(112)
MD11	3.0×10^{14}	2.5×10^{14}	3.64	(112)

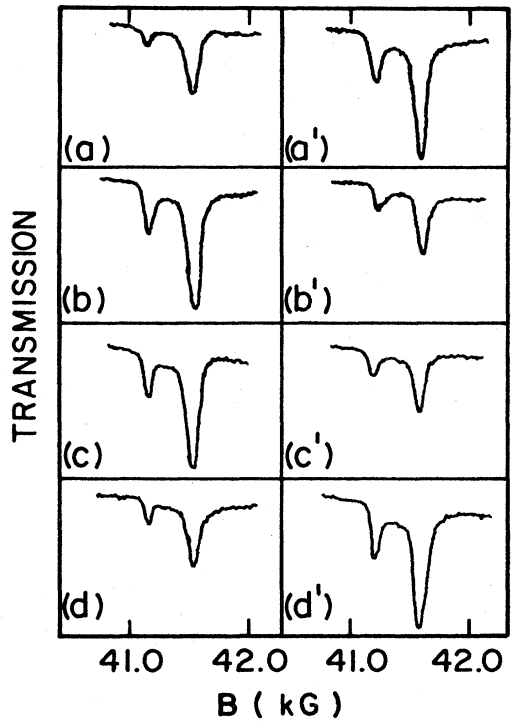

FIG. 4. Symmetry characteristics of spin resonance in n-InSb, observed on sample MD7 in the parallel Voigt geometry at 118.8 μm and 4.5 K. (a) spin resonance for $\mathbf{B}_0||[1\bar{1}0]$, $\mathbf{q}||[110]$; (b) the sample was rotated by 180° about $\mathbf{q}$ relative to (a); (c) the sample was rotated by 180° about $\mathbf{B}_0$ relative to (a); (d) the sample was rotated by 180° about $\mathbf{q}\times\mathbf{B}_0$ relative to (a). The sequence (a')—(d') corresponds to configurations (a)—(d), respectively, but with the magnetic field reversed. In each resonance doublet the higher-field, stronger line is the conduction-electron spin resonance, and the weaker line is spin resonance of donor-bound electrons.

(1) The intensity of SR changes quite strongly (by a factor of about 2) when the direction of the magnetic field is reversed relative to the crystallographic directions. This is observed by reversing the field itself [compare, e.g., Figs. 4(a) and 4(a')] or by rotating the sample by 180° about $\mathbf{q}$ while keeping $\mathbf{B}_0$ fixed in the laboratory frame [compare Figs. 4(a) and 4(b)].

(2) It is easily shown that rotating the sample by 180° about $\mathbf{B}_0$ is equivalent to reversing the direction of $\mathbf{q}$ relative to the crystallographic directions, while keeping $\mathbf{B}_0$ fixed relative to the crystal frame. A change in SR intensity similar to that which takes place on reversing $\mathbf{B}_0$ is observed when $\mathbf{q}$ is reversed in this manner [compare Figs. 4(a) and 4(c)].

(3) Rotating the sample about $\mathbf{q}\times\mathbf{B}_0$ is equivalent to reversing the direction of both $\mathbf{q}$ and $\mathbf{B}_0$ with respect to the sample. This operation leaves the SR intensity unchanged [compare Fig. 4(a) with Fig. 4(d); Fig. 4(a') with Fig. 4(d')].

We have carried out SR measurements on all the specimens listed in Table I, which also includes samples with (100), (111), and (112) faces. All these samples contain at least one $[1\bar{1}0]$ direction (or equivalent) in the sample plane, facilitating comparison. When $\mathbf{B}_0$ was parallel to the $[1\bar{1}0]$ in the case of the (111) and (112) samples, a similar asymmetry was observed with respect to field reversal and/or sample rotation as that shown in Fig. 4. The results for the (100) samples were unique, however, in that for this case the dependence of SR on reversing of $\mathbf{B}_0$ or $\mathbf{q}$ vanished. This is completely consistent with the analysis of the EDMD interference described in Sec. II. This result can also be understood on intuitive grounds. In the case of a slab with (100) faces, a 180° rotation about $\mathbf{q}$ (i.e., about the [100] direction) leaves the InSb crystal microscopically invariant, as can easily be seen by performing this operation on a laboratory model of the zinc-blende lattice. Since in the Voigt geometry such a rotation is equivalent to changing the sign of the magnetic field with respect to the sample frame, any effect related to reversing the magnetic field in this plane must vanish.

We found the EDMD interference effects described above to be very reproducible in all the samples studied, with various electron concentrations, thicknesses, and orientations. The effects occurred as an inseparable part of the EDSR in the parallel Voigt geometry at all temperatures ($2.0<T<35$ K) and FIR wavelengths ($96.5<\lambda<251.1$ μm) where the experiments were performed. Additional evidence that the EDMD interference effect is a basic property of the material is provided by the study of how this effect depends on the direction of the magnetic field with respect to the zinc-blende lattice in *absolute* terms. Since—as has been pointed out in Sec. III—in InSb it is possible to distinguish physically between the [111] and $[\bar{1}\bar{1}\bar{1}]$ directions by appropriate etching, we were able to ascertain that the EDMD interference effects observed in different samples were consistent among themselves. For example, SR intensity was strong for $\mathbf{B}_0||[1\bar{1}0]$, $\mathbf{q}||[112]$ and weak for $\mathbf{B}||[\bar{1}10]$, $\mathbf{q}||[112]$ in *all* (112) samples.

Spin-resonance measurements were also carried out for all the above samples in CRA and CRI circular polarizations in the Faraday geometry, as well as in the perpendicular Voigt geometry ($\mathbf{E}\perp\mathbf{B}_0$). We found that the EDMD interference effects disappear in all these configurations, i.e., spin resonance does not depend on reversing $\mathbf{B}_0$ or $\mathbf{q}$ (in the case of CRA and CRI, on simultaneously reversing $\mathbf{B}_0$ and the sense of circular polarization). Again, this is consistent with theoretical predictions.

As we have mentioned in Sec. II, the dependence of the resonance intensity on reversing $\mathbf{B}_0$ provides a convenient way of obtaining the inversion asymmetry parameter δ_0. The ratio of the absorption coefficients for $\mathbf{B}_0$ parallel and antiparallel to $[1\bar{1}0]$ in the (110) plane obtained at 118.8 μm is 1.96 ± 0.07. Using Eq. (29), we then calculate $\delta_0=56\pm3$ a.u. or $(3.6\pm0.2)\times10^{-34}$ erg cm^3. Here we have used $g=43.25$ obtained at 118.8 μm (i.e., at 41.5 kG) from the present measurements, and the refractive index $n=4.1$ from the work of Dixon *et al.*[12] Rashba and Sheka[3] have estimated the value of δ_0 to be of the order of 200 a.u., but they point out that this estimate may differ significantly from the true value. Also K. Sugihara[13] estimated δ_0 in InSb to be 100 a.u. by fitting the linewidth of microwave spin-resonance data. We believe that the

value of δ_0 obtained in our measurements is the best determination of this parameter to date.

B. Angular dependence of spin-resonance absorption in OV geometry

We have examined the anisotropy of the spin-resonance intensity over 360°, which not only provides detailed information on the angular dependence of the resonance, but also ascertains that there exist no preferred directions other than those associated with the crystal symmetry in the samples (e.g., there are no strains). Spin-resonance absorption coefficients observed in the parallel Voigt geometry as a function of orientation of $\mathbf{B}_0$ in the (100) plane (sample MD8), (110) plane (sample MD7), (111) plane (sample MD9), and (112) plane (sample MD1) are shown in Figs. 5 , 6 , 7, and 8, respectively. The measurements were performed at 118.8 μm and 4.5 K. Note the strong angular dependence of the data, and (with the exception of Fig. 5) the systematic difference of the absorption coefficients corresponding to opposite field directions, indicated by solid and open circles, respectively. The theoretical curves are obtained by adjusting the magnitude of the electric-dipole and magnetic-dipole resonance intensities in Eqs. (28), (32), (39), and (40) (i.e., by adjusting the value of δ_0), with the solid and dashed curves drawn for opposite directions of $\mathbf{B}_0$. It is to be emphasized that the *same* value $\delta_0=56$ a.u. was used to fit *all* data. The bottom straight line in Figs. 5—8 shows the intensity of the magnetic-dipole spin resonance that would be observed if EDSR were absent. The results for the (100) sample are unique in that for this case the EDMD

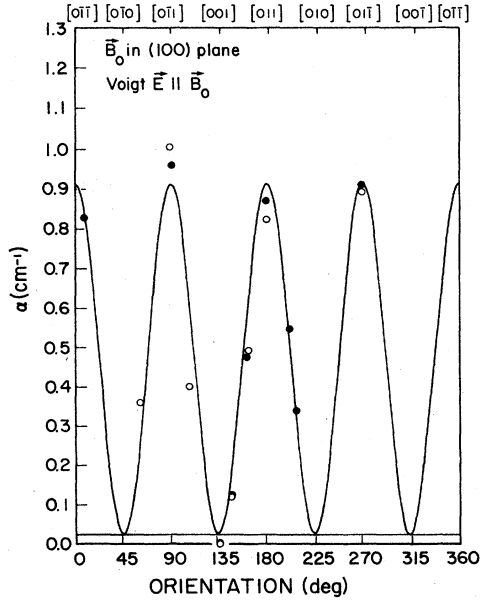

FIG. 5. Spin-resonance absorption coefficient of conduction electrons in n-InSb for the OV geometry as a function of orientation of $\mathbf{B}_0$ in the (100) plane. Solid and open circles correspond to opposite signs of $\mathbf{B}_0$, respectively. The solid curve is the theoretical angular dependences fitted to the experimental data. The horizontal line near zero shows the calculated intensity of the magnetic-dipole spin resonance alone. The data were taken on sample MD8 at 118.8 μm and 4.5 K.

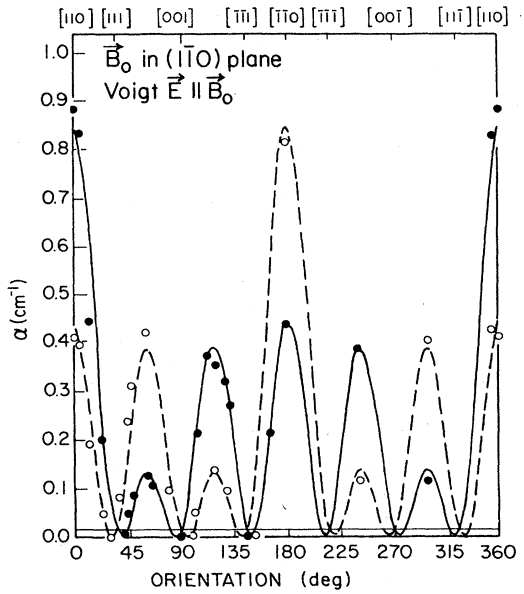

FIG. 6. Spin-resonance absorption coefficient of conduction electrons in n-InSb for the OV geometry as a function of orientation of $\mathbf{B}_0$ in the (1$\bar{1}$0) plane. Solid and open circles correspond to opposite signs of $\mathbf{B}_0$, respectively. The solid and dashed curves are the theoretical angular dependences fitted to the experimental data for opposite field directions. The horizontal line near zero shows the calculated intensity of the magnetic-dipole spin resonance alone. The data were taken on sample MD7 at 118.8 μm and 4.5 K. Note that at the point where the solid and dashed curves cross, α is determined entirely by magnetic-dipole absorption.

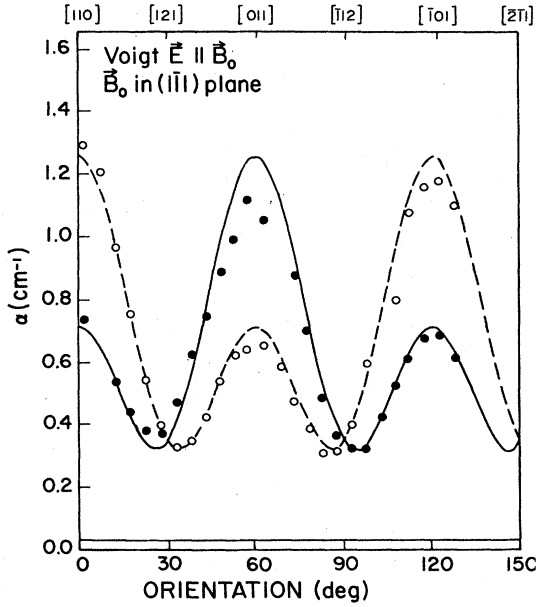

FIG. 7. Spin-resonance absorption coefficient of conduction electrons in n-InSb as a function of orientation of $\mathbf{B}_0$ in the (1$\bar{1}$1) plane. Solid and open circles correspond to opposite signs of $\mathbf{B}_0$, respectively. The solid and dashed curves are the theoretical angular dependences fitted to the experimental data for opposite field directions. The horizontal line near zero shows the calculated intensity of the magnetic-dipole spin resonance alone. The data were taken on sample MD9 at 118.8 μm and 4.5 K.

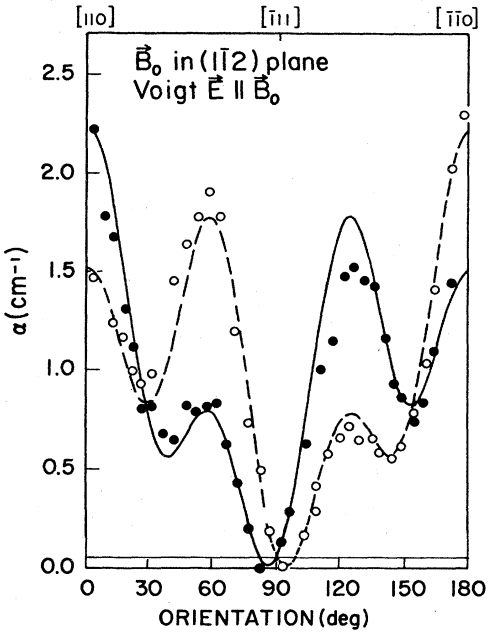

FIG. 8. Spin-resonance absorption coefficient of conduction electrons in n-InSb as a function of orientation of $\mathbf{B}_0$ in the (1$\bar{1}$2) plane. Solid and open circles correspond to opposite signs of $\mathbf{B}_0$, respectively. The solid and dashed curves are the theoretical angular dependences fitted to the experimental data for opposite field directions. The horizontal line near zero shows the calculated intensity of the magnetic-dipole spin resonance alone. The data were taken on sample MD1 at 118.8 μm and 4.5 K. At the point where the solid and dashed curves cross EDSR = 0, and α is determined entirely by the magnetic-dipole contribution.

interference vanishes for all orientations of $\mathbf{B}_0$, as shown in Fig. 5. For the other planes the agreement between experimental and theoretical angular dependence of the SR absorption coefficient (Figs. 6—8) provides an excellent demonstration of the existence of EDMD interference in the spin-resonance absorption in zinc-blende semiconductors.

C. Effect of inversion asymmetry on electric-dipole spin resonance

As has already been pointed out, electric-dipole-excited spin resonance (EDSR) is allowed in the presence of spin-orbit coupling by one or more of the following mechanisms: wave-function mixing through $\mathbf{k}\cdot\mathbf{p}$ interaction ("nonparabolicity"), inversion asymmetry, or warping. Of these only inversion asymmetry is predicted to allow EDSR in the parallel Voigt (OV) geometry.[2,3] This prediction is fully verified by the excellent agreement between the inversion-asymmetry-based analysis of Sec. II and the experimentally observed anisotropy of spin resonance for the OV configuration.

In addition to the measurements in the OV geometry, we have also investigated spin resonance in the Faraday configuration (for both CRA and CRI polarizations) and in the perpendicular Voigt (EV) configuration. Comparison between EDSR intensities for the Faraday and the OV geometries for three samples with similar electron concentrations is shown in Table II. "Zero" in the table indicates that the resonance, if present, was too weak to be detected. We also list, in Table III, the mechanisms and incident polarizations which allow the EDSR transition when $\mathbf{B}_0$ is applied along principal crystal directions (after Ref. 3). On the basis of Tables II and III we conclude that inversion asymmetry is in fact the dominant mechanism allowing EDSR in InSb in *all* configurations. This can be seen as follows.

(1) Having established that EDSR in the OV geometry is exclusively due to inversion asymmetry, we note from Table II that the intensity of the OV resonance is *much stronger* than in the other configurations (where in principle other mechanisms could also allow EDSR).

(2) As can be seen from Table III, nonparabolicity is a possible mechanisms for EDSR only in the CRI geometry. We exclude it as the principal mechanisms even in that configuration, because nonparabolicity-induced EDSR is expected to be isotropic, contrary to the data in Table II. Our data for the EV geometry (which is in effect a superposition of CRI and CRA contributions) is also highly anisotropic, confirming that the principal mechanism of EDSR for $\mathbf{E}\perp\mathbf{B}_0$ is strongly angle dependent.

(3) Comparison of Tables II and III also eliminates warping as the chief mechanism of EDSR. Warping contribution to EDSR occurs only for CRA and is anisotropic, with maximum intensity for $\mathbf{B}_0\|[110]$ and zero for $\mathbf{B}_0\|[100]$. The observed EDSR, on the other hand, vanishes for $\mathbf{B}_0\|[110]$ and is maximum for $\mathbf{B}_0\|[100]$ in the CRA geometry.

(4) While the observed anisotropy disagrees completely with the behavior expected for nonparabolicity- and warping-induced EDSR, it is in excellent agreement with the theoretical predictions for inversion asymmetry in all the configurations studied.

These arguments of course do not exclude the possibility that the other mechanisms also contribute weakly to EDSR. Indeed, data for InSb samples with $N\simeq 4\times 10^{15}$

TABLE II. Relative EDSR intensities in various geometries.

Sample No.	Carrier Concentration (cm^{-3})	Orientation	Absorption coefficient (cm^{-1}) CRA	CRI	Voigt $\mathbf{E}\|\|\mathbf{B}_0\|\|[110]$
MD7	2.3×10^{14}	(110)	0	0	0.65
MD8	3.6×10^{14}	(100)	0.07	0	0.86
MD9	4.5×10^{14}	(111)	0	0.18	1.27

TABLE III. Selection rules for EDSR in zinc-blende crystals induced by inversion asymmetry (IA), nonparabolicity ($\mathbf{k}\cdot\mathbf{p}$), and warping ($W$). [From M. H. Weiler, R. L. Aggarwal, and B. Lax, Phys. Rev. B 17, 3269 (1978).]

	CRA			CRI			Parallel Voigt		
	IA	$\mathbf{k}\cdot\mathbf{p}$	W	IA	$\mathbf{k}\cdot\mathbf{p}$	W	IA	$\mathbf{k}\cdot\mathbf{p}$	W
$\mathbf{B}_0\|\|[100]$	yes	no	no	no	yes	no	no	no	no
$\mathbf{B}_0\|\|[110]$	no	no	yes	no	yes	no	yes	no	no
$\mathbf{B}_0\|\|[111]$	no	no	no	yes	yes	no	no	no	no

cm^{-3} show a weak resonance in the CRI polarization for $\mathbf{B}_0||[100]$ and $\mathbf{B}_0||[110]$ which, according to Table III, can only be ascribed to nonparabolicity. This resonance, however, is invariably much weaker than in any geometry where EDSR is allowed by inversion asymmetry. Thus we are forced to conclude that—at least in the range of electron concentrations and magnetic fields involved in these experiments—inversion asymmetry is by far the most important mechanism for allowing the observation of EDSR in n-InSb.

ACKNOWLEDGMENTS

The authors are grateful to Sudha Gopalan for valuable comments, and to N. Samarth for carrying out the microwave helicon measurements of electron concentration in the InSb samples. This work was supported by the National Science Foundation through Grant No. DMR-82-18783. We also acknowledge the use of the Purdue Central Laser Facility supported by NSF-MRL Grant No. DMR-83-16988.

APPENDIX: MACROSCOPIC APPROACH TO EDMD INTERFERENCE, ONSAGER RELATIONS, AND TIME REVERSAL

The frequency-dependent dielectric response tensor $\overleftrightarrow{\epsilon}(\omega,\mathbf{B}_0)$ is not sufficient to describe the $\mathbf{B}_0$ and $\mathbf{q}$ dependence described above. This can be seen from the Onsager relations, which require that

$$\epsilon_{ij}(\omega,\mathbf{B}_0)=\epsilon_{ji}(\omega,-\mathbf{B}_0)\ . \tag{A1}$$

Since the dielectric response in the parallel Voigt ($\mathbf{E}||\mathbf{B}_0$) geometry (for $\mathbf{B}||\hat{\mathbf{z}}$) is described by ϵ_{zz}, Eq. (A1) as it stands immediately implies that the spectra cannot depend on the *sign* of $\mathbf{B}_0$, which is contrary to observation. This suggests that, to describe the observed results, we must generalize the dielectric tensor to include first-order terms in wave vector $\mathbf{q}$, i.e., we must use the *nonlocal* form of the response function, $\overleftrightarrow{\epsilon}(\omega,\mathbf{q},\mathbf{B}_0)$. In this case the Onsager relations require that

$$\epsilon_{ij}(\omega,\mathbf{q},\mathbf{B}_0)=\epsilon_{ji}(\omega,-\mathbf{q},-\mathbf{B}_0) \neq\epsilon_{ij}(\omega,\mathbf{q},-\mathbf{B}_0)=\epsilon_{ji}(\omega,-\mathbf{q},\mathbf{B}_0)\ . \tag{A2}$$

As a consequence of including $\mathbf{q}$, the diagonal components of $\overleftrightarrow{\epsilon}$ thus acquire a dependence on the sign of $\mathbf{q}$ or $\mathbf{B}_0$.

To examine the nonlocal contribution to the dielectric response function for crystals with T_d symmetry (zinc-blende crystals), we first write $\epsilon_{ij}(\omega,\mathbf{q},\mathbf{B}_0)$ in a power series,[14]

$$\epsilon_{ij}(\omega,\mathbf{q},\mathbf{B}_0)=\epsilon_{ij}(\omega)+i\gamma_{ij}q_l+\alpha_{ijl}B_l+\beta_{ijlm}B_lq_m+\cdots\ . \tag{A3}$$

Here we will concentrate on the term $\beta_{ijlm}B_lq_m$, because it exists only when the crystal lacks a center of inversion, and because it depends on the sign of $\mathbf{B}_0$ or $\mathbf{q}$. These are the exact properties which we have described in the preceding section for the spin-resonance spectra. We can rewrite β_{ijlm} as

$$\beta_{ijlm}=\tfrac{1}{2}(\beta_{ijlm}+\beta_{ijml})+\tfrac{1}{2}(\beta_{ijlm}-\beta_{ijml}) =\beta^{(S)}_{ijlm}+\beta^{(A)}_{ijlm}\ . \tag{A4}$$

It can be shown that $\beta^{(A)}_{ijlm}$ can be represented in the form[14]

$$\beta^{(A)}_{ijlm}=\epsilon_{lmn}C_{nij}\ , \tag{A5}$$

where ϵ_{lmn} is the antisymmetric unit matrix, and C_{nij} is an ordinary tensor of rank three, $C_{nij}=C_{nji}$. The symmetry properties of tensor C_{nij} are exactly the same as those of the tensor characterizing the piezoelectric effect. Thus,

$$\beta^{(A)}_{ijlm}B_lq_m=C_{nij}\epsilon_{lmn}B_lq_m =C_{nij}(\mathbf{B}_0\times\mathbf{q})_n\ . \tag{A6}$$

For crystals belonging to T_d symmetry, the nonvanishing components of the tensor C_{nij} are the following:[14]

$$C_{123}=C_{231}=C_{312}=C_{132}=C_{213}=C_{321}=\eta\ , \tag{A7}$$

all of which are equal to some value η. $\beta^{(A)}_{ijlm}B_lq_m$ can then be written as

$$\beta^{(A)}_{ijlm}B_lq_m=\eta\begin{bmatrix} 0 & (\mathbf{B}_0\times\mathbf{q})_3 & (\mathbf{B}_0\times\mathbf{q})_2 \\ (\mathbf{B}_0\times\mathbf{q})_3 & 0 & (\mathbf{B}_0\times\mathbf{q})_1 \\ (\mathbf{B}_0\times\mathbf{q})_2 & (\mathbf{B}_0\times\mathbf{q})_1 & 0 \end{bmatrix}\ . \tag{A8}$$

The contribution of $\beta^{(A)}_{ijlm}B_lq_m$ to the dielectric response in the OV geometry for an arbitrary orientation of $\mathbf{B}_0$ is obtained by a coordinate transformation of Eq. (A8) from the cubic crystal axes to a coordinate frame where $\hat{\mathbf{z}}||\mathbf{B}_0$, yielding

$$\Delta\epsilon_{\mathrm{OV}}=2\eta[\sin\theta\cos\theta\sin\phi(\mathbf{B}_0\times\mathbf{q})_1+\sin\theta\cos\theta\cos\phi(\mathbf{B}_0\times\mathbf{q})_2 +\sin^2\theta\cos\phi\sin\phi(\mathbf{B}_0\times\mathbf{q})_3]\ , \tag{A9}$$

where θ and ϕ are the polar angle and the aximuth, respectively, of $\mathbf{B}_0$. The results of the angular dependence of $\Delta\epsilon_{OV}$ for $\mathbf{B}_0$ in the (100), (110), (111), and (112) planes are given as follows. For $\mathbf{B}_0$ in the (100) plane

$$\Delta\epsilon_{OV}=0 , \tag{A10}$$

for $\mathbf{B}_0$ in the (110) plane

$$\Delta\epsilon_{OV}=\eta B_0 q \sin\theta(2\cos^2\theta-\sin^2\theta) , \tag{A11}$$

for $\mathbf{B}_0$ in the (111) plane

$$\Delta\epsilon_{OV}=\frac{1}{\sqrt{3}}\eta B_0 q[\sin^3\theta\sin(2\phi)(\cos\phi+\sin\phi) + \sin\theta\sin(2\theta)\cos^2\phi - 2\cos^2\theta\sin\theta(\cos\phi+\sin\phi)] , \tag{A12}$$

and for $\mathbf{B}_0$ in the (112) plane

$$\Delta\epsilon_{OV}=\frac{1}{\sqrt{6}}\eta B_0 q[-\sin^3\theta\sin(2\phi)(\sin\phi+\cos\phi) - 2\sin\theta\sin(2\theta)\cos^2\phi + 2\sin\theta\cos^2\theta(\sin\phi+\cos\phi)] . \tag{A13}$$

Comparing Eqs. (A10)—(A13) with the interference term in Eqs. (28), (32), (39), and (40), we find that the angular dependence is exactly the same. Since the relationship between the imaginary part of the dielectric response function and the absorption coefficient is

$$\alpha=\frac{\epsilon''\omega}{cn} , \tag{A14}$$

the coefficient η contained in the elements of the tensor C_{nij} is therefore equal to

$$\eta=6\frac{\delta_0 e^2 g\beta_0\pi N}{\hbar^3\omega^2\gamma} . \tag{A15}$$

For the Faraday geometry, we have $\mathbf{B}_0||\mathbf{q}$. We can thus see immediately from Eq. (A6) that the contribution of the term $\beta^{(A)}_{ijlm}B_l q_m$ vanishes. Again, this is consistent with the disappearance of the EDMD interference in that geometry. For the perpendicular Voigt geometry, the contribution of $\beta^{(A)}_{ijlm}B_l q_m$ to the dielectric response is given by

$$\Delta\epsilon_{\perp}=-\eta[\sin\theta\cos\theta\sin\phi(\mathbf{B}_0\times\mathbf{q})_1+\sin\theta\cos\theta\cos\phi(\mathbf{B}_0\times\mathbf{q})_2 + \sin^2\theta\sin\phi\cos\phi(\mathbf{B}_0\times\mathbf{q})_3] . \tag{A16}$$

Thus, if there simultaneously existed both electric and magnetic-dipole transitions, then from symmetry arguments for the zinc-blende structure the dielectric response function of the EDMD interference would be described by the above angular behavior. If, however, one of the dipole transitions vanishes, the parameter η must vanish, and the contribution of $\beta^{(A)}_{ijlm}B_l q_m$ to the dielectric response must also disappear. Again, this is exactly the case for the spin resonance in the $\mathbf{E}\perp\mathbf{B}_0$ geometry.

From the above analysis we therefore conclude that EDMD interference is equivalent to a nonlocal contribution (i.e., to an explicit contribution of the photon momentum) to the dielectric response function.

*Present address: Division of Applied Sciences, Harvard University, Cambridge, MA 02138.

†On leave from the Institute of Physics of the Polish Academy of Sciences, 02-668 Warszawa, Poland.

[1]Y. Yafet, in *Solid State Physics,* edited by F. Seitz and D. Turnbull (Academic, New York, 1963), Vol. 14, p. 1; V. I. Sheka, Fiz. Tverd. Tela **6**, 3099 (1964) [Sov. Phys.—Solid State **6**, 2470 (1965)].

[2]E. I. Rashba and V. I. Sheka, Fiz. Tver. Tela **3**, 1735 (1961); **3**, 1863 (1961) [Sov. Phys.—Solid State **3**, 1257 (1961); **3**, 7357 (1961)].

[3]M. H. Weiler, R. L. Aggarwal, and B. Lax, Phys. Rev. B **17**, 3269 (1978).

[4]B. D. McCombe and R. J. Wagner, Phys. Rev. B **4**, 1285 (1975).

[5]A preliminary report on these effect was published by M. Dobrowolska, Y.-F. Chen, J. K. Furdyna, and S. Rodriguez, Phys. Rev. Lett. **51**, 134 (1983).

[6]N. R. Ogg, Proc. Phys. Soc. **89**, 431 (1966).

[7]M. Dobrowolska, A. Witowski, J. K. Furdyna, T. Ichiguchi, H. D. Drew, and P. A. Wolff, Phys. Rev. Lett. **49**, 845 (1982); Phys. Rev. B **29**, 6652 (1984).

[8]Y. F. Chen, Ph.D. thesis, Purdue University, 1984 (unpublished).

[9]J. K. Furdyna, Rev. Sci. Instrum. **37**, 462 (1966).

[10]J. W. Allen, Philos. Mag. **2**, 1475 (1957).

[11]J. W. Faust, Jr. and A. Sagar, J. Appl. Phys. **31**, 331 (1960).

[12]J. R. Dixon, Jr. and J. K. Furdyna, Solid State Commun. **35**, 195 (1980).

[13]K. Sugihara, J. Phys. Soc. Jpn. **38**, 1061 (1975).

[14]V. M. Agranovich and V. L. Ginzburg, *Crystal Optics with Spatial Dispersion, and Excitons,* Vol. 42 of *Springer Series in Solid State Sciences* (Springer, Berlin, 1984), pp. 133 and 196.